

Research paper

DRAC: Dose Rate and Age Calculator for trapped charge dating

Julie A. Durcan^{a, *}, Georgina E. King^{b, c, *}, Geoffrey A.T. Duller^c^a School of Geography and the Environment, University of Oxford, South Parks Road, Oxford, OX1 3QY, UK^b Institute of Earth Surface Dynamics, University of Lausanne, Bâtiment Geopolis, UNIL-Mouline, 1015 Lausanne, Switzerland^c Department of Geography and Earth Sciences, Aberystwyth University, Aberystwyth, Ceredigion, SY23 3DB, UK

ARTICLE INFO

Article history:

Received 5 December 2014

Received in revised form

26 March 2015

Accepted 30 March 2015

Available online 31 March 2015

Keywords:

DRAC

Dose rate

Age

Calculator

Luminescence dating

Electron spin resonance dating

Software

Open access

ABSTRACT

Accurate calculation of the environmental radiation dose rate (\dot{D}) is an essential part of trapped charge dating methods, such as luminescence and electron spin resonance dating. Although the calculation of \dot{D} is not mathematically complex, the incorporation of multiple variables and the propagation of uncertainties can be challenging. The Dose Rate and Age Calculator (DRAC) is an open access, web-based program which enables rapid \dot{D} calculation for trapped charge dating applications. Users can select from recently published attenuation and conversion factors to make mathematically robust, reproducible \dot{D} calculations. Comparison of DRAC calculated \dot{D} values against the published \dot{D} determinations of 422 samples from 32 studies results in a reproducibility ratio of 1.01 ± 0.05 . It is anticipated that DRAC will facilitate easier inter-laboratory comparisons and will provide greater transparency for \dot{D} calculations. DRAC will be updated to reflect the latest advances in \dot{D} calculation and is freely accessible at www.aber.ac.uk/alrl/drac. The code for DRAC is available from github at <https://github.com/DRAC-calculator/DRAC-calculator>.

© 2015 Elsevier B.V. All rights reserved.

1. Introduction

Trapped charge dating techniques such as luminescence and electron spin resonance (ESR) dating are key Quaternary dating methods and in a period of 22 months from January 2013, over 500 papers have been published using these techniques. Within luminescence dating, calculation of the environmental dose rate (\dot{D}) is equally important as calculation of the equivalent dose (D_e) in age determinations, yet many luminescence dating publications tend to be more focused upon the calculation of D_e values. The recent luminescence laboratory inter-comparison project (Buylaert et al., 2006; Murray et al., in press) initially reported at the UK Luminescence meeting held in Aberystwyth in September 2012, highlighted that whilst D_e values are measured reproducibly between different laboratories, greater variability is seen in \dot{D} determinations. This may be partly explained by the variety of measurement techniques used to infer \dot{D} , i.e. some laboratories use

techniques to determine radionuclide concentrations (e.g. inductively-coupled plasma mass spectrometry (ICP-MS)), whereas other laboratories use emission counting methods to directly measure radioactivity. However, De Corte et al. (2007) compared a wide range of different methods for dose rate determination and did not record major differences between techniques. An alternative explanation is variability in the parameters used in \dot{D} determinations, such as different radionuclide conversion factors (e.g. Adamiec and Aitken, 1998; Guerin et al., 2012) and dose rate attenuation factors (e.g. Brennan, 2003; Mejdahl, 1979), which will result in minor variability in the calculated \dot{D} . Furthermore, although the mathematics required in the dose rate calculation is not complex, the compilation of in excess of 10 variables (Fig. 1) provides many opportunities for miscalculation. To overcome the challenges of \dot{D} calculation, desktop based programs have been previously published e.g. the AGE program (Grün, 2009). However as this program is written to be run in a DOS based language it requires additional DOS emulation software to run in versions of Windows more recent than XP and the radionuclide conversion factors it uses have now been superseded. Other programs have not been formally published (e.g. ADELE; Kulig, 2005) and are not widely available. We present here a web-based Dose Rate and Age

* Corresponding authors.

E-mail addresses: julie.durcan@ouce.ox.ac.uk (J.A. Durcan), georgina.king@gmail.com (G.E. King).

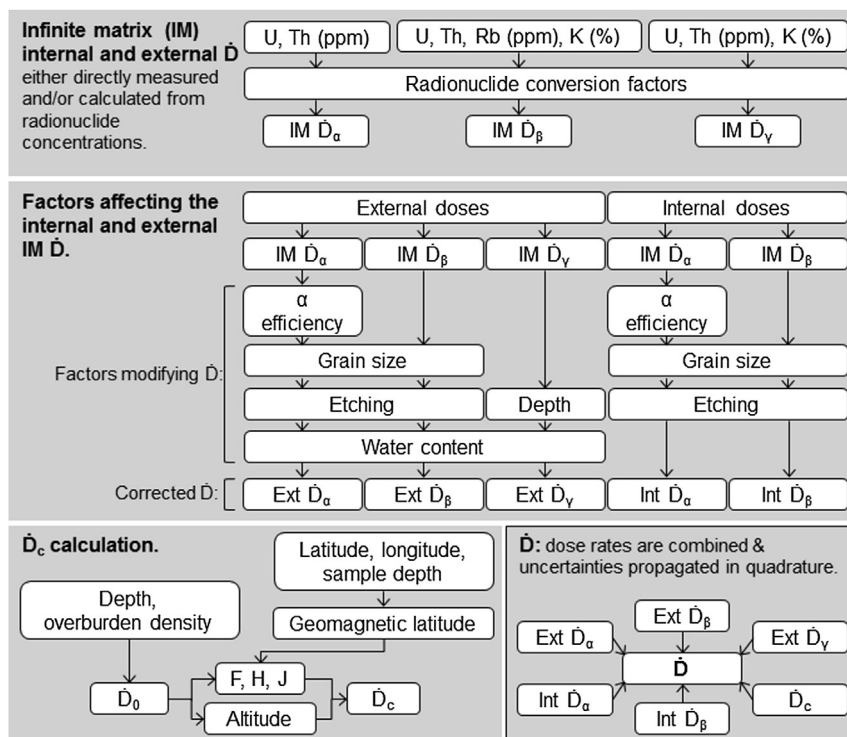


Fig. 1. Overview of the \dot{D} calculation for trapped charge dating applications. IM – infinite matrix, ext – external, int – internal.

Calculator (DRAC), which is freely available and can be more easily updated to reflect the most recent conversion and attenuation factor publications. By providing a standardised calculator with transparent calculations which utilises published input variables, DRAC provides an effective means of removing the potential for miscalculation and will facilitate improved assessment of dose rate and age calculations and more simple inter-laboratory \dot{D} comparisons.

2. DRAC website and data input

DRAC (v1.1) can be accessed at www.aber.ac.uk/alrl/drac and is hosted by the Aberystwyth Luminescence Research Laboratory, Aberystwyth University, UK. The publication of DRAC as a website ensures that users will immediately benefit from software updates, and that revised inputs can be rapidly incorporated into the calculation code. A key objective of DRAC is calculation transparency, and it is intended that all users will be able to easily trace the methods used to calculate published dose rate values in a similar manner to the cosmogenic nuclide dating community, who have recently benefitted from the development of CRONUS (Balco et al., 2008). Therefore, the DRAC calculation code is listed on github which is an open access code repository, and can be accessed using a link from the DRAC website.

The DRAC website is comprised of three key parts: a user guide, the calculator input page, and the data tables summary. The user guide page provides a short introduction to the calculation process used by DRAC and provides a summary of the inputs required and outputs generated by DRAC. On the calculator input page, users can download a .csv template of the inputs required for the dose rate calculation, and once this has been populated, can copy and paste their data into the calculation box. Note that because this comprises a text input, it is important to ensure that values are input with the correct number of significant figures. DRAC users can input data for

multiple samples by populating multiple rows of data, facilitating the rapid analysis of a number of samples simultaneously. Once users click “calculate”, DRAC produces an output file in .csv format which provides a summary table, as well as listing all of the inputs used, the variables that have been selected (e.g. a-value, grain size etc.) and calculated values (e.g. the different attenuation factors). Input and output tables populated with example data are provided in the [Supplementary Information](#) for reference, although users should always refer to the DRAC website to ensure they are using the most up to date versions of the input and output tables. The data tables page provides the datasets (e.g. conversion factors, attenuation factors) that can be selected and used in the \dot{D} calculation. These datasets are also detailed in the [Supplementary Information](#).

3. Determination of the environmental dose rate (\dot{D})

Four types of radiation contribute to the \dot{D} received by a sample: alpha particles (α), beta particles (β), gamma rays (γ) and cosmic rays. The dose rate from each of these sources is combined to calculate the total \dot{D} , which is used in trapped charge dating calculations. The alpha (\dot{D}_α), beta (\dot{D}_β) and gamma (\dot{D}_γ) dose rates originate from naturally occurring radionuclides, including Uranium (U), Thorium (Th) and Potassium (K), which are present in the surrounding sediment matrix and make up a proportion of the crystalline structure of some minerals. The radiation emitted can be attenuated due to a variety of factors including grain size and sediment-matrix water content, requiring that dose rates are adjusted. The cosmic dose rate (\dot{D}_c) received by a sample is a function of the geographic location, burial depth and altitude from which the sample was taken. In DRAC, the internal and external dose rates are calculated and attenuated as appropriate, and along with the \dot{D}_c , these are combined to calculate the total \dot{D} . The calculation stages are discussed below.

3.1. External alpha, beta and gamma dose rates

Aitken (1985a) comments that for the majority of samples, U, Th and K comprise almost all of the total \dot{D} in approximately equal parts, with a small contribution from Rubidium (Rb) and the D_c . Dose rates resulting from the decay of these elements can be calculated either by determining the radionuclide concentrations present in the sediment matrix or by directly measuring the emission of radiation from the sediment (cf. De Corte et al., 2007). Many measurement techniques are available for dose rate determination, including ICP-MS, neutron activation analysis, gamma spectrometry, thick source alpha and beta counting, and alpha spectroscopy.

DRAC offers the flexibility of inputting either radionuclide concentrations and/or directly measured dose rates. Alternatively, a combination of the two can be used, e.g. the \dot{D}_β may be measured directly using beta counting, whilst the \dot{D}_α and \dot{D}_γ are determined from radionuclide concentrations. Where the user inputs a combination of radionuclide concentrations and directly measured dose rates, DRAC will use the specified dose rate in calculations. These specified dose rates should be input in $\text{Gy}\cdot\text{ka}^{-1}$, and will be attenuated by DRAC in subsequent calculation stages. Users will note from Table S1 that radionuclide concentrations of U, Th and Rb should be input in ppm and K in %. Details of how to convert from $\text{Bq}\cdot\text{kg}^{-1}$ to ppm and $\text{K}_2\text{O}\%$ to K are detailed in the Supplementary Information (Table S3.1). Where the user opts to use radionuclide concentrations for dose rate calculations, they have the option of either inputting a Rb concentration or deriving Rb from the K concentration, where Rb (ppm) is equal to $-9.17 + 38.13 \text{ K} (\%)$ after Mejdahl (1987).

3.1.1. Radionuclide conversion factors

A set of conversion factors are used to calculate the infinite-matrix alpha, beta and gamma dose rates derived from a radionuclide. Conversion factors for each radionuclide derived from nuclear data tables have been published by a number of authors (e.g. Adamiec and Aitken, 1998). Liritzis et al. (2013) have most recently updated the conversion factors from values previously published by Guerin et al. (2011) and Adamiec and Aitken (1998). In contrast to previous contributions, Liritzis et al. (2013) have also calculated uncertainties for their conversion factors and in the absence of calculated uncertainties in the studies of Guerin et al. (2011) and Adamiec and Aitken (1998), proportional uncertainties derived from Liritzis et al. (2013) are applied to all three datasets. The data tables used in DRAC can be viewed in the Supplementary Information accompanying this paper (Table S3.2) and on the DRAC website. Radionuclide concentrations are multiplied by the relevant conversion factor to determine the \dot{D}_α , \dot{D}_β and \dot{D}_γ delivered by the decay of each element. The uncertainties are propagated in quadrature when calculating the dose rate from each of the radionuclides. Further details of the calculation process and worked examples are presented in the Supplementary Information (S3.9, S3.10, and S3.11).

3.2. Internal alpha and beta dose rates

The inclusion of U, Th and K within the mineral lattice of quartz and feldspar grains results in an internal \dot{D}_α and \dot{D}_β component, which is particularly significant for K-feldspars. For quartz, Aitken (1998) suggests that in most environments, the contribution of the internal alpha dose rate to the \dot{D} is negligible, particularly given its low alpha efficiency (Rees-Jones and Tite, 1997). However, in some environments with low environmental dose rates, internal doses for quartz may account for a few percent of the total dose rate (e.g. Armitage and King, 2013; Jacobs et al., 2003; Sutton and

Zimmerman, 1978). Users of DRAC working in low dose environments can incorporate a user-defined and attenuated internal \dot{D} within their dose rate calculation (e.g. Vandenberghe et al., 2008) if required. The inclusion of K within the structure of K-feldspars results in an internal \dot{D}_β (e.g. Huntley and Baril, 1997) and the recent development of the post-IR IRSL protocol (Buylaert et al., 2009; Thomsen et al., 2008) and technological advances that facilitate single-grain K-feldspar dating, have resulted in efforts to precisely measure individual-grain internal K contents (e.g. Smedley et al., 2012). In DRAC, users should input a K concentration value for their samples or may wish to use the K content values of $12.5 \pm 0.5\%$ of Huntley and Baril (1997) or the $10 \pm 2\%$ measured by Smedley et al. (2012).

In DRAC, users can input internal radionuclide concentrations of U, Th and K which will be multiplied by the selected conversion factors to calculate the internal \dot{D}_α and \dot{D}_β , and which will be adjusted for grain size. The internal \dot{D}_α will also be adjusted for alpha efficiency. Alternatively, users may input a specified internal \dot{D} ($\text{Gy}\cdot\text{ka}^{-1}$) which should be the sum of both the internal \dot{D}_α and \dot{D}_β , user defined internal dose rates, and must be provided in a grain-size attenuated form, because without specified radionuclide concentrations it is not possible for DRAC to calculate an appropriate attenuation factor.

3.3. Attenuation factors

In order to determine the \dot{D} from the calculated internal and external \dot{D}_α , \dot{D}_β and \dot{D}_γ , it is necessary to adjust the doses for a range of factors, including alpha efficiency, grain size, removal of the grain surface by etching, and moisture content. DRAC users can select from a variety of published datasets for attenuation of dose rates, as detailed below.

3.3.1. Alpha efficiency (a-value)

In contrast to beta particles and gamma rays, alpha particles are highly ionising and cause the saturation of trapping defects within their alpha decay tracks (Aitken, 1985a). This is corrected for by using an alpha efficiency factor, or a-value (Aitken and Bowman, 1975), which can be considered as the ratio of luminescence per unit alpha track length to the luminescence per unit absorbed beta dose (Aitken, 1985b). A range of a-values have been published in the literature for different grain-sizes and mineral types, and within DRAC, users should input their selected a-value for any samples where an alpha contribution is to be calculated. The most commonly used published values include 0.15 ± 0.05 for coarse-grained K-feldspar (Balescu and Lamothe, 1994), 0.10 ± 0.02 for coarse-grained quartz (Olley et al., 1998), 0.038 ± 0.002 for fine-grained quartz (Rees-Jones, 1995) and 0.086 ± 0.004 for poly-mineral fine grains (Rees-Jones, 1995), but see also Lai et al. (2008), Lang (1994), Mauz et al. (2006) and Spooner et al. (1990) for other values. If an a-value is provided, the user defined external \dot{D}_α , or the dose rate calculated from U and Th concentrations will be adjusted accordingly.

3.3.2. Grain size

The range of alpha and beta particles may be comparable with the diameter of the grains under investigation, therefore dose rates must be corrected for grain-size attenuation effects. Bell (1980) calculated attenuation factors for alpha dose rates from U and Th for quartz, and more recently Brennan et al. (1991) calculated alpha attenuation factors for spherical grains, accounting for alpha track length. The attenuation factors of Brennan et al. (1991) are greater than those of Bell (1980) (Fig. 2), however as the factors of Bell (1980) have remained in widespread use throughout OSL publications over the past ~30 years, users may select from either set of

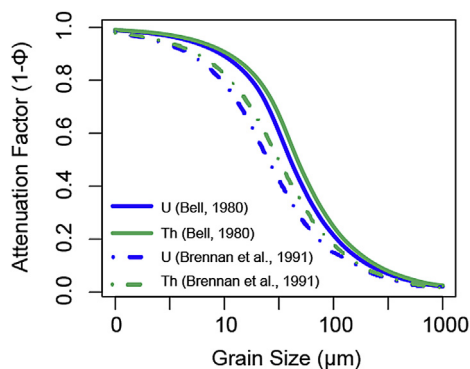


Fig. 2. Grain size attenuation factors for \dot{D}_α , interpolated from the original data of Bell (1980) and Brennan et al. (1991) using a spline fit. The original and fitted data are available in Tables S3.3a and S3.3b.

attenuation factors in DRAC. For \dot{D}_β grain size attenuation, DRAC users can choose between four datasets: Mejdahl (1979), Brennan (2003), and Guerin et al. (2012) who offer two sets of factors, one for quartz and one for feldspar (Fig. 3). If a Rb concentration has been provided or calculated, the dataset of Readhead (2002a,b) will be used to attenuate the \dot{D}_β from Rb. The different sets of attenuation factors assume grain sphericity, infinite matrix homogeneity and radionuclide equilibrium.

Each of the grain size attenuation datasets has been fitted with a smoothed spline function in RStudio, and datasets have been generated over the grain size range 1–1000 μm . The original and fitted data are provided in the Supplementary Information (Tables S3.3a,b and S3.4a,b). The fitted alpha and beta grain size attenuation factors are summarised in Figs. 2 and 3 respectively. The attenuation factors ($1 - \Phi(D)$) are used to correct external doses, whilst the absorption factors ($\Phi(D)$) are used for internal doses.

Using the grain size data provided by the user, DRAC calculates the attenuation factor from the minimum and maximum grain size

and takes the mean as the grain size attenuation or absorption factor. Quantification of the uncertainties associated with each of the attenuation factor datasets is not discussed in the various studies, although Brennan (2003) comments that there is a likely uncertainty of several percent for his modelled data, but does not provide a numerical uncertainty estimate. In DRAC, the uncertainty is calculated from half of the absolute difference between the attenuation factors of the minimum and maximum grain sizes.

The decay of radionuclides within the U, Th and K series produce emissions of various energies, and therefore the degree of attenuation by the grain varies according to the relative contributions from these different sources. In DRAC, dose rates are calculated from radionuclide concentrations and conversion factors, or the user can specify a directly measured dose rate. Where radionuclide concentrations (U, Th, K) have been provided, the dose rate arising from each radionuclide is attenuated individually, before being summed to produce the attenuated \dot{D}_α or \dot{D}_β . If user-defined \dot{D}_α and \dot{D}_β values are provided, an average attenuation factor calculated assuming the elemental ratios of Mejdahl (1979) (3 ppm U, 12 ppm Th, 1% K_2O) is used. If no conversion factors have been stipulated because only user defined doses have been provided, DRAC will default to using the most recent conversion factors of Liritzis et al. (2013).

3.3.3. Chemical etching

Chemical etching using hydrofluoric acid is routinely used in the preparation of quartz extracts, both to remove contaminating grains and to remove the majority of the alpha irradiated outer grain margin. It is generally assumed that etching results in removal of an isotropic surface (e.g. Fleming, 1970), however experimental results from Bell and Zimmerman (1978) showed that etching was not uniform for a large proportion of the grains explored (75%) and in some instances resulted in the formation of deep etch pits. Some coarse-grain feldspar preparation protocols also include a chemical etch for the same reason (e.g. Li et al., 2008), although feldspars are known not to etch isotropically (Duller, 1992). Consequently,

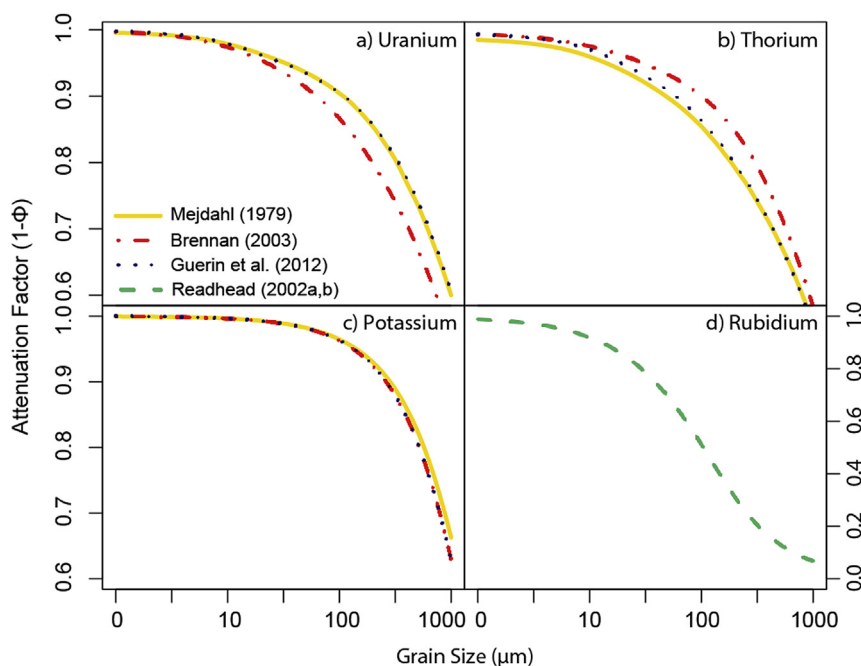


Fig. 3. Grain size attenuation factors for \dot{D}_β , interpolated from the original data of Mejdahl (1979), Brennan (2003), Guerin et al. (2012) and Readhead (2002a,b). Note that only the quartz factors of Guerin et al. (2012) are shown, but both the quartz and feldspar factors are available for use within DRAC. The original and fitted data are available in Tables S3.4a and S3.4b.

applying any etch attenuation factor is subject to uncertainty. Bell (1979) and Brennan (2003) have calculated the change in \dot{D}_β caused by chemical etching for quartz grains for a range of etch depths. The factors of Bell (1979) are reported as a ratio to the grain size attenuated absorbed dose, and thus can be regarded as secondary etch attenuation factors ($1 - \Phi_{2e}$). In contrast the factors of Brennan (2003) are reported as independent etch attenuation factors ($1 - \Phi_e$) which do not require additional grain size attenuation. To make the different sets of etch attenuation factors comparable, the 100 μm factors of Brennan (2003) are expressed as secondary attenuation factors, achieved through scaling them relative to the 100 μm grain-size attenuation factors also reported in Brennan (2003). At present both of the available secondary etch attenuation factors in DRAC assume an initial grain size of 100 μm , although it should be noted that Brennan (2003) provides factors for a range of grain sizes.

Users of DRAC should provide a sample etch depth range (in μm) and can use the secondary beta etch attenuation factors of either Bell (1979) or Brennan (2003). These datasets have been fitted with a smoothing spline function (Ripley, 2013) over a range of 1–30 μm in RStudio (Tables S3.5a,b and S3.6a,b), and are used to further attenuate the \dot{D}_β . The uncertainties associated with etch depth attenuation are not discussed by either Bell (1979) or Brennan (2003), and therefore in DRAC, the uncertainty is calculated from half of the absolute difference between the attenuation factors of the minimum and maximum etch depths. Combined secondary etch attenuation factors have also been calculated from the data of Brennan (2003) and Bell (1979) using the elemental ratios of Mejdahl (1979). Note that as Bell (1979) comments that the beta dose from K is negligibly affected by chemical etching, no K etch attenuation is incorporated for the Bell (1979) combined etch attenuation factors. The effect of chemical etching on the beta dose from Rb is not considered although Bell (1979) notes that for an etch of 9 μm depth, the beta dose of Rb is reduced by a factor of 0.755.

Alpha particles penetrate grains of quartz and feldspar to a lesser depth than beta particles. Consequently, the \dot{D}_α is more seriously reduced following chemical etching, and commonly it is assumed that the \dot{D}_α has been completely removed by chemical etching. If users wish to completely ignore any remaining alpha contribution following chemical etching, zero should be input for the a-value. If the a-value is non-zero then the \dot{D}_α remaining following chemical etching will be calculated using the secondary etch attenuation factors of Bell (1979), which are also subject to an assumed grain size of 100 μm . The later factors of Brennan et al. (1991) are not included in DRAC because of limited resolution over the 1–30 μm etch depth range.

3.3.4. Scaling of the gamma dose rate

Conventional sampling strategies for trapped charge dating suggest avoiding sample collection from within 0.3 m of the current sediment surface, which is the range of gamma rays. In near-surface settings the \dot{D}_γ should be corrected to take into account the gamma contribution from the sediment matrix, as well as the inert atmosphere above ground level. DRAC offers the option of correcting the \dot{D}_γ calculated for samples collected from depths of 0.3 m or less using the scaling factors of Aitken (1985a, b; Table S3.7). For samples within 0.3 m of the surface, the \dot{D}_γ from U, Th and K will be individually scaled, unless a user specified \dot{D}_γ is provided, in which case the weighted average scaling factor computed by Aitken is applied.

3.3.5. Water content

Water has significant attenuating properties. External \dot{D}_α , \dot{D}_β and \dot{D}_γ must therefore be adjusted for the water content of the

sediment from which the sample was taken over the burial lifetime of the sample. The attenuation factors of Aitken and Xie (1990) and Zimmerman (1971) are used in the DRAC calculation, and are 1.49, 1.25 and 1.14 for alpha, beta and gamma radiation respectively. Dose rates are attenuated using the equation of Aitken and Xie (1990) and uncertainties are propagated in quadrature. The water content and uncertainty should be expressed as a percentage and be the weight of water divided by dry sediment: water (%) by mass = (wet mass – dry mass/dry mass) \times 100.

3.4. Cosmic dose rate

The contribution from cosmic rays to the total environmental dose rate, whilst small in most depositional settings, is not negligible (Prescott and Hutton, 1994) and should be included as part of the environmental dose rate. The \dot{D}_c calculation is detailed in Prescott and Hutton (1988, 1994) and DRAC uses the calculation protocol outlined in the appendix of Prescott and Hutton (1994; p. 500). Barbouti and Rastin (1983) observed that the soft component of cosmic rays only penetrates shallow depths of up to 167 $\text{g}\cdot\text{cm}^{-2}$ (Fig. 4). At greater depths, the \dot{D}_c comprises only the hard (muon) component. In DRAC, the contribution from the soft and hard component will be calculated for samples taken from depths between 0 and 167 $\text{g}\cdot\text{cm}^{-2}$. At greater depths, only the hard component is calculated (Fig. 4). For \dot{D}_c calculation, DRAC requires the input of the sample depth and the mean overburden density to calculate the \dot{D}_c at a geomagnetic latitude of 55° and 0 m asl. This dose rate is then corrected for the sample-specific geomagnetic latitude and altitude, and users are required to include the latitude, longitude and altitude of the sampling location. Users of DRAC can find a worked example of this calculation in Worksheets S3.9, S3.10, S3.11, along with the look-up table of F, H and J values (Table S3.8) required to correct for location (e.g. Prescott and Stephan, 1982; Prescott and Hutton, 1994) in the Supplementary Information and on the DRAC website.

Cosmic dose rates may fluctuate over longer-term time-scales, due to variability in galactic primary cosmic rays, solar modulation and changes in the geomagnetic dipole moment, although this variability is likely to have averaged out over the past 500 ka (Prescott and Hutton, 1994). To account for possible fluctuations and uncertainties associated with the production of cosmic rays over time, DRAC applies an uncertainty of $\pm 10\%$ to calculated \dot{D}_c values. For more complex depositional settings, users of DRAC also

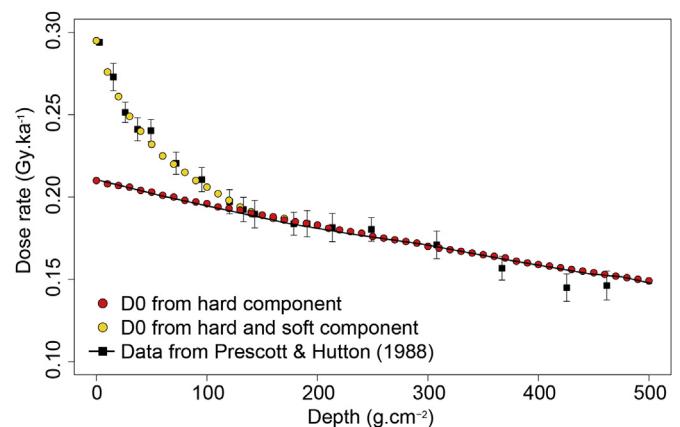


Fig. 4. Penetration depths of cosmic rays. The original data from Barbouti and Rastin (1983) as presented in Prescott and Hutton (1988) are shown, together with their fit for the hard component. Data fitted for this study for the contributions from both soft and hard components (depths < 167 $\text{g}\cdot\text{cm}^{-2}$) and from hard components only (depths > 167 $\text{g}\cdot\text{cm}^{-2}$) are shown.

have the option of inputting a user defined \hat{D}_c .

3.5. Calculation of \hat{D} and age

\hat{D} is calculated by combining the attenuated internal and external \hat{D}_α and \hat{D}_β , the attenuated \hat{D}_γ and the \hat{D}_c . The values are combined and uncertainties propagated in quadrature. DRAC will also calculate an age if a D_e and uncertainty have been provided, where $\text{age} = D_e/\hat{D}$.

4. DRAC comparison

Worked examples of the calculation of DRAC for quartz, feldspar and polymineral samples are provided in the [Supplementary Information \(Worksheets S3.9, S3.10 and S3.11\)](#), along with the DRAC Input and DRAC Output tables (worksheets S3.12 and S3.13). To test \hat{D} values calculated by DRAC against published dose rates, \hat{D} information was taken from 32 randomly selected studies (totalling 422 samples) and used to calculate \hat{D} in DRAC (v1.1). For the 32 studies selected it was necessary to estimate some parameters where they were not detailed in the publication e.g. if the conversion factors used were not stated, the factors of [Adamiec and Aitken \(1998\)](#) were used. Full details of the assumptions made are given in the caption of [Fig. 5](#), which summarises the comparison, presented according to mineral type and grain size. For the full dataset of 422 samples, DRAC and published \hat{D} values are in excellent agreement with a ratio of 1.01 ± 0.05 . This demonstrates that as a community, \hat{D} values are calculated consistently, although some small deviation

between DRAC and published \hat{D} values is to be expected because of the small variations which will arise from the use of different conversion factors and/or attenuation datasets, some of which have had to be assumed. Sensitivity testing of a quartz sample from [Durcan \(2012\)](#) shows that a $\pm 2\%$ variation around the calculated value can be generated through the use of different conversion factors, attenuation factors, sample location parameters and uncertainties. Transposition and miscalculation errors have been observed in some publications, which again, leads to discrepancy between the published and DRAC calculated \hat{D} values. Despite these various factors, the deviation from unity is slight.

4.1. Reporting \hat{D} calculation

The 32 publications used for the DRAC comparison comprises a small proportion of the number of studies investigated for inclusion. This is because the vast majority of publications reviewed did not contain enough basic information to reproduce the \hat{D} calculation. We as authors do not wish to dictate a standardised set of data which should be included in journal publications. However, we do ask the community to be mindful of the information necessary to reproduce a \hat{D} calculation and to incorporate these details in their publications (or [supplementary information](#)) accordingly.

5. Future directions

DRAC is intended to provide a robust and accessible method of dose rate calculation, which enables practitioners to accurately

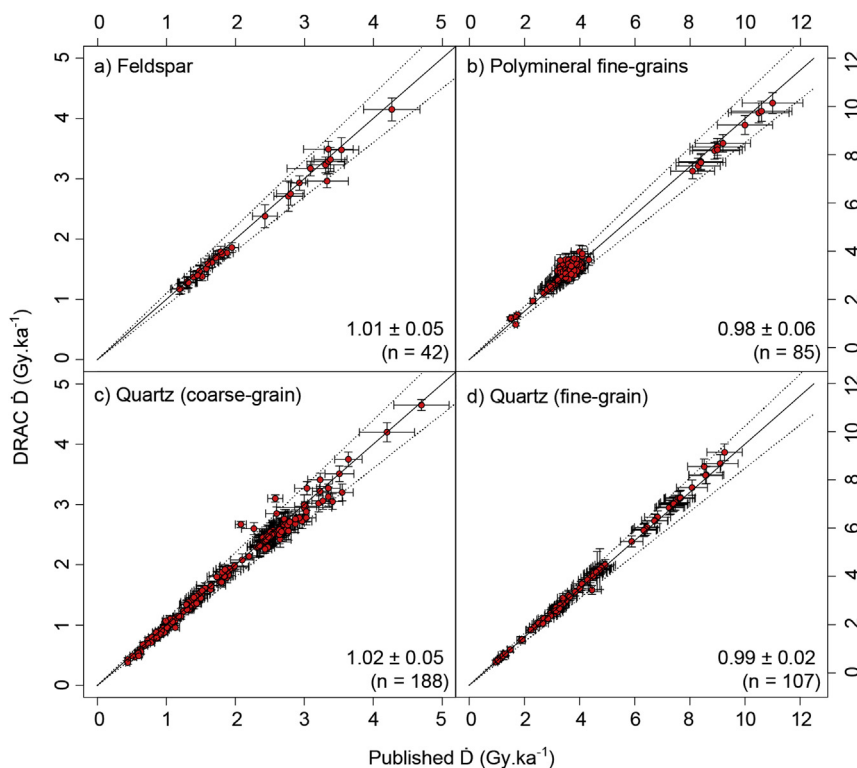


Fig. 5. Comparison of dose rates (\hat{D}) calculated in DRAC with those previously published. Data are plotted separately for a) feldspar, b) polymineral, c) coarse-grain ($>63 \mu\text{m}$) quartz and d) fine-grain ($<63 \mu\text{m}$) quartz. 422 samples from 32 studies are compared with a mean ratio of 1.01 ± 0.05 . If not stated in the publication, the following parameters were used to facilitate comparison: conversion factors – [Adamiec and Aitken \(1998\)](#), no Rb calculation from K, grain size attenuation for \hat{D}_α and \hat{D}_β – [Bell \(1980\)](#) and [Mejdahl \(1979\)](#) respectively, etch depth – $9 \mu\text{m}$, etch depth attenuation – [Bell, 1979](#), a-value either 0.086 ± 0.0043 , 0.035 ± 0.001 ([Rees-Jones and Tite, 1997](#)) or 0.15 ± 0.015 ([Balescu and Lamothe, 1994](#)) dependent on mineral and grain-size, overburden density – $2.0 \pm 0.1 \text{ g.cm}^{-3}$, latitude, longitude and altitude estimated from Google Earth. The studies used for the DRAC comparison: [Alappat et al. \(2011\)](#), [Bates et al. \(2003\)](#), [Bremner et al. \(2003\)](#), [Buylaert et al. \(2007\)](#), [Clark-Balzan et al. \(2012\)](#), [Davidovich et al. \(2012\)](#), [Demeter et al. \(2012\)](#), [Fuchs et al. \(2012\)](#), [Haberzettl et al. \(2009\)](#), [Halfen et al. \(2010\)](#), [Hall et al. \(2010\)](#), [Houben et al. \(2013\)](#), [Kaiser et al. \(2009\)](#), [Kars et al. \(2012\)](#), [Kels et al. \(2014\)](#), [Klasen et al. \(2011\)](#), [Kock et al. \(2009\)](#), [Kreutzer et al. \(2012\)](#), [Le Dortz et al. \(2009\)](#), [Lepper et al. \(2013\)](#), [Lomax et al. \(2013\)](#), [Lomax et al. \(2014\)](#), [Madsen et al. \(2009\)](#), [Roskosch et al. \(2012\)](#), [Schatz et al. \(2012\)](#), [Schmidt et al. \(2014\)](#), [Schokker et al. \(2005\)](#), [Stevens et al. \(2011\)](#), [Tamura et al. \(2011\)](#), [Thiel et al. \(2011\)](#), [Xu et al. \(2010\)](#), [Yang et al. \(2010\)](#).

determine environmental dose rates. The website calculations are intended to be transparent and to enable interested parties to recalculate published environmental dose rate values reproducibly. Users may refer to the [Supplementary Information](#) and/or DRAC website for an outline of the DRAC calculations and worked examples. It is anticipated that DRAC will facilitate easier inter-laboratory comparisons of environmental dose rate values, through the standardisation of dose rate calculations.

Rather than comprising a final version, it is intended that DRAC will undergo modification as advances in environmental dose rate calculations are made. Potential extensions to the calculator could include the incorporation of Monte-Carlo modelling for beta dose heterogeneity (e.g. Nathan et al., 2003), calculation of gamma dose heterogeneity or the extension of the calculator to other minerals such as calcite. Contributions to DRAC are welcomed and DRAC users are encouraged to contact the authors with updated dose rate datasets, such as conversion and attenuation factors, and/or potential developments to the calculator.

Acknowledgements

Funding from the Quaternary Research Association Outreach Fund has supported the development of this website, and Aberystwyth University is gratefully acknowledged for hosting. JD is supported by the School of Geography and the Environment, University of Oxford. GK acknowledges financial support from the Climate Change Consortium of Wales and Swiss National Fund grant PP00P2-38956. Barry Brennan is thanked for providing his attenuation factor data. Stefan Senk at Senktec (www.senktec.com) designed and built the DRAC website and is thanked for his expertise and creativity. Richard Bailey, Rachel Smedley and participants at the 14th Luminescence and Electron Spin Resonance Dating Conference are thanked for fruitful discussion and suggestions. Corresponding authors JD and GK contributed equally to writing of the manuscript and development of the calculator.

Appendix A. Supplementary data

Supplementary data related to this article can be found at <http://dx.doi.org/10.1016/j.quageo.2015.03.012>.

References

- Adamiec, G., Aitken, M.J., 1998. Dose-rate conversion factors: update. *Anc. TL* 16, 37–46.
- Aitken, M.J., 1985a. *Thermoluminescence Dating*. Academic Press, London.
- Aitken, M.J., 1985b. Alpha particle effectiveness: numerical relationship between systems. *Anc. TL* 3, 22–25.
- Aitken, M.J., 1998. *An Introduction to Optical Dating: the Dating of Quaternary Sediments by the Use of Photon-stimulated Luminescence*. Oxford Science Publications, Oxford.
- Aitken, M.J., Bowman, S.G.E., 1975. Thermoluminescent dating: assessment of alpha particle contribution. *Archaeometry* 17, 132–138.
- Aitken, M.J., Xie, J., 1990. Moisture correction for annual gamma dose. *Anc. TL* 8, 6–9.
- Alappat, L., Frechen, M., Ramesh, R., Tsukamoto, S., Srinivasulu, S., 2011. Evolution of late Holocene coastal dunes in Cauvery delta region of Tamil Nadu, India. *J. Asian Earth Sci.* 42, 381–397.
- Armitage, S.J., King, G.E., 2013. Optically stimulated luminescence dating of hearths from the Fazzan Basin, Libya: a tool for determining the timing and pattern of Holocene occupation of the Sahara. *Quat. Geochronol.* 15, 88–97.
- Balco, G., Stone, J.O., Lifton, N.A., Dunai, T.J., 2008. A complete and easily accessible means of calculating surface exposure ages or erosion rates from ¹⁰Be and ²⁶Al measurements. *Quat. Geochronol.* 3, 174–195.
- Balescu, S., Lamothe, M., 1994. Comparison of TL and IRSL age estimates of feldspar coarse grains from waterlain sediments. *Quat. Sci. Rev.* 13, 437–444.
- Barbouth, A.I., Rastin, B.C., 1983. A study of the absolute intensity of muons at sea level and under various thicknesses of absorber. *J. Phys. G: Nucl. Phys.* 9, 1577–1595.
- Bates, M., Pope, M., Shaw, A., Scott, B., Schwenninger, J.-L., 2003. Late Neanderthal occupation in North-West Europe: rediscovery, investigation and dating of a last glacial sediment sequence at the site of La Cotte de Saint Brelade, Jersey. *J. Quat. Sci.* 28, 647–652.
- Bell, W.T., 1979. Attenuation factors for the absorbed radiation dose in quartz inclusions for thermoluminescence dating. *Anc. TL* 8, 1–12.
- Bell, W.T., 1980. Alpha attenuation in Quartz grains for Thermoluminescence Dating. *Anc. TL* 12, 4–8.
- Bell, W.T., Zimmerman, D.W., 1978. The effect of HF acid etching on the morphology of quartz inclusions for thermoluminescence dating. *Archaeometry* 20, 63–65.
- Breman, E., Gillson, L., Willis, K., 2003. How fire and climate shaped grass-dominated vegetation and forest mosaics in northern South Africa during past millennia. *Holocene* 22, 1427–1439.
- Brennan, B.J., 2003. Beta doses to spherical grains. *Radiat. Meas.* 37, 299–303.
- Brennan, B.J., Lyons, R.G., Phillips, S.W., 1991. Attenuation of alpha particle track dose for spherical grains. *Int. J. Radiat. Appl. Instrum. Part D. Nucl. Tracks Radiat. Meas.* 18, 249–253.
- Buylaert, J.-P., Vandenberghe, D., Murray, A.S., Huot, S., De Corte, F., Van den Haute, P., 2007. Luminescence dating of old (>70 ka) Chinese loess: a comparison of single-aliquot OSL and IRSL techniques. *Quat. Geochronol.* 2, 9–14.
- Buylaert, J., Ankjaergaard, C., Murray, A.S., Nielsen, A., 2006. A Proposed Laboratory Intercomparison Sample Based on a Beach-Ridge Sand From Skagen (Denmark). UK Luminescence and ESR Meeting, Liverpool, UK.
- Buylaert, J.P., Murray, A.S., Thomsen, K.J., Jain, M., 2009. Testing the potential of an elevated temperature IRSL signal from K-feldspar. *Radiat. Meas.* 44, 560–565.
- Clark-Balzan, L.A., Candy, I., Schwenninger, J.-L., Bouzouggar, A., Blockley, S., Nathan, R., Barton, R.N.E., 2012. Coupled U-series and OSL dating of a Late Pleistocene cave sediment sequence, Morocco, North Africa: significance for constructing Palaeolithic chronologies. *Quat. Geochronol.* 12, 53–64.
- Davidovich, U., Porat, N., Gadot, Y., Avni, Y., Lipschits, O., 2012. Archaeological investigations and OSL dating of terraces at Ramat Rahel, Israel. *J. Field Archaeol.* 37, 192–208.
- De Corte, F., Vandenberghe, D., Hossain, S.M., De Wispelaere, A., Buylaert, J.-P., Van den Haute, P., 2007. Preparation and characterization of loess sediment for use as a reference material in the annual radiation dose determination for luminescence dating. *J. Radioanal. Nucl. Chem.* 272 (2), 311–319.
- Demeter, F., Shackelford, L.L., Bacon, A.-M., Düringer, P., Westaway, K., Sayavongkhamdy, T., Braga, J., Sichanthongtip, P., Khamdalavong, P., Ponche, J.-L., Wang, H., Lundström, C., Patole-Edoumba, E., Karpoff, A.-M., 2012. Anatomically modern human in Southeast Asia (Laos) by 46 ka. *Proc. Natl. Acad. Sci.* 109, 14375–14380.
- Duller, G.A.T., 1992. *Luminescence Chronology of Raised Marine Terraces, South-West North Island, New Zealand*. Unpublished PhD thesis. University of Wales, Aberystwyth.
- Durcan, J.A., 2012. *Luminescence Dating of Sediments in Punjab, Pakistan: Implications for the Collapse of the Harappan Civilisation*. Unpublished PhD thesis. Aberystwyth University.
- Fleming, S.J., 1970. Thermoluminescent dating: refinement of the quartz inclusion method. *Archaeometry* 12, 133–143.
- Fuchs, M., Kreutzer, S., Fischer, M., Sauer, D., Sørensen, R., 2012. OSL and IRSL dating of raised beach sand deposits along the southeastern coast of Norway. *Quat. Geochronol.* 10, 195–200.
- Guerin, G., Mercier, N., Adamiec, G., 2011. Dose-rate conversion factors: update. *Anc. TL* 29, 5–8.
- Guerin, G., Mercier, N., Nathan, R., Adamiec, C., Lefrais, Y., 2012. On the use of the infinite matrix assumption and associated concepts: a critical review. *Radiat. Meas.* 47, 778–785.
- Grün, 2009. The “AGE” program for the calculation of luminescence age estimates. *Anc. TL* 27, 45–46.
- Haberzettl, T., Anselmetti, F.S., Bowen, S.W., Fey, M., Mayr, C., Zolitschka, B., Ariztegui, D., Mauz, B., Ohlendörfer, C., Kastner, S., Lucke, A., Schabitz, F., Wille, M., 2009. Late Pleistocene dust deposition in the Patagonian steppe – extending and refining the palaeoenvironmental and tephrochronological record from Laguna Potrok Aike back to 55 ka. *Quat. Sci. Rev.* 28, 2927–2939.
- Halfen, A.F., Gredlund, G.G., Mahan, S.A., 2010. Holocene stratigraphy and chronology of the Casper Dune Field, Casper, Wyoming, USA. *Holocene* 29, 773–783.
- Hall, S.A., Miller, M.R., Goble, R.J., 2010. Geochronology of the Bolson sand sheet, New Mexico and Texas, and its archaeological significance. *Geological Soc. Am. Bull.* 122, 1950–1967.
- Houben, P., Köhl, N., Dambeck, R., Overath, J., 2013. Lateglacial to Holocene rapid crater infilling of a MIS 2 maar volcano (West-Eifel Volcanic Field, Germany): environmental history and geomorphological feedback mechanisms. *Boreas* 42, 947–958.
- Huntley, D.J., Baril, M.R., 1997. The K content of the K-feldspars being measured in optical dating or in thermoluminescence dating. *Anc. TL* 15, 11–13.
- Jacobs, Z., Wintle, A.G., Duller, G.A.T., 2003. Optical dating of dune sand from Blombos Cave, South Africa: I—multiple grain dating. *J. Hum. Evol.* 44, 599–612.
- Kaiser, K., Lai, Z., Schneider, B., Schoch, W.H., She, X., Miede, G., Brückner, H., 2009. Sediment sequences and paleosols in the Kyichu Valley, southern Tibet (China), indicating Late Quaternary environmental changes. *Isl. Arc* 18, 404–427.
- Kars, R.H., Busschers, F.S., Wallinga, J., 2012. Validating post IR-IRSL dating on K-feldspars through comparison with quartz OSL ages. *Quat. Geochronol.* 12, 74–86.
- Kels, H., Protze, J., Sitlivy, V., Hilgers, A., Zander, A., Anghelinu, M., Bertrams, M., Lehmkuhl, F., 2014. Genesis of loess-like sediments and soils at the foothills of the Banat Mountains, Romania – examples from the Paleolithic sites Românești and Coșava. *Quat. Int.* 351, 213–230.

- Klasen, N., Engle, M., Bruckner, H., Hausleiter, A., Intilia, A., Eichmann, R., Al-Najem, M.H., Al-Said, S.F., 2011. Optically stimulated luminescence dating of the city wall system of ancient Tayma (NW Saudi Arabia). *J. Archaeol. Sci.* 38, 1818–1826.
- Kock, S., Huggenberger, P., Preusser, F., Rentzel, P., Wetzel, A., 2009. Formation and evolution of the Lower Terrace of the Rhine River in the area of Basel. *Swiss J. Geosci.* 102, 307–321.
- Kreutzer, S., Fuchs, M., Meszner, S., Faust, D., 2012. OSL chronostratigraphy of a loess-palaeosol sequence in Saxony/Germany using quartz of different grain sizes. *Quat. Geochronol.* 10, 102–109.
- Kulig, G., 2005. Erstellung einer Auswertesoftware zur Altersbestimmung mittels Lumineszenzverfahren unter spezieller Berücksichtigung des Einflusses radioaktiver Ungleichgewichte in der 238U-Zerfallsreihe (Creation of a software for luminescence dating with special attention to the influence of radioactive disequilibria in the 238U decay chain) (Technische Bergakademie Freiberg, Freiberg unpublished BSc thesis).
- Lai, Z.P., Zöller, L., Fuchs, M., Brückner, H., 2008. Alpha efficiency determination for OSL of quartz extracted from Chinese loess. *Radiat. Meas.* 43, 767–770.
- Lang, A., 1994. Infra-red stimulated luminescence dating of Holocene reworked silty sediments. *Quat. Geochronol.* 13, 525–528.
- Le Dortz, K., Meyer, B., Sebrier, M., Nazari, H., Braucher, R., Fattahi, M., Benedetti, L., Foroutan, M., Sime, L., Bourles, D., Talebian, M., Bateman, M.D., Ghorashi, M., 2009. Holocene right-slip rate determined by cosmogenic and OSL dating on the Anar fault, Central Iran. *Geophys. J. Int.* 179, 700–710.
- Lepper, K., Buell, A.W., Fisher, T.G., Lowell, T.V., 2013. A chronology for glacial Lake Agassiz shorelines along Upham's namesake transect. *Quat. Res.* 80, 88–98.
- Li, B., Li, S.-H., Wintle, A.G., Zhao, H., 2008. Isochron dating of sediments using luminescence of K-feldspar grains. *J. Geophys. Res. Earth Surf.* 113, F02026.
- Liritzis, I., Stamoulis, K., Papachristodoulou, C., Ioannides, K., 2013. A re-evaluation of radiation dose-rate conversion factors. *Mediterr. Archaeol. Archaeom.* 13, 1–15.
- Lomax, J., Fuchs, M., Preusser, F., Fiebig, M., 2014. Luminescence based loess chronostratigraphy of the Upper Palaeolithic site Krems-Wachtberg, Austria. *Quat. Int.* 351, 88–97. <http://dx.doi.org/10.1016/j.quaint.2012.10.037>.
- Madsen, A.T., Duller, G.A.T., Donnelly, J.P., Roberts, H.M., Wintle, A.G., 2009. A chronology of hurricane landfalls at Little Sippewissett Marsh, Massachusetts, USA, using optical dating. *Geomorphology* 109, 36–45.
- Mauz, B., Packman, S., Lang, A., 2006. The alpha effectiveness in silt-sized quartz: new data obtained by single and multiple aliquot protocols. *Anc. TL* 24, 47–52.
- Mejdahl, V., 1979. Thermoluminescence dating: beta-dose attenuation in quartz grains. *Archaeometry* 21, 61–72.
- Mejdahl, V., 1987. Internal radioactivity in quartz and feldspar grains. *Anc. TL* 5, 10–17.
- Murray, A., Buylaert, J.-P., Thiel, C., 2015. A luminescence dating intercomparison based on a Danish beach-ridge sand. *Radiat. Meas.* (in press).
- Nathan, R.P., Thomas, P.J., Jain, M., Murray, A.S., Rhodes, E.J., 2003. Environmental dose rate heterogeneity of beta radiation and its implications for luminescence dating: Monte Carlo modelling and experimental validation. *Radiat. Meas.* 37, 305–313.
- Olley, J., Caitcheon, G., Murray, A., 1998. The distribution of apparent dose as determined by Optically Stimulated Luminescence in small aliquots of fluvial quartz: Implications for dating young sediments. *Quat. Sci. Rev.* 17, 1033–1040.
- Prescott, J.R., Hutton, J.T., 1988. Cosmic ray and gamma ray dosimetry for TL and ESR. *Nucl. Tracks Radiat. Meas.* 14, 223–227.
- Prescott, J.R., Hutton, J.T., 1994. Cosmic ray contributions to dose rates for luminescence and ESR dating: large depths and long-term time variations. *Radiat. Meas.* 23, 497–500.
- Prescott, J.R., Stephan, L.G., 1982. The contribution of cosmic radiation to the environmental dose for thermoluminescence dating. *PACT* 6, 17–25.
- Readhead, M.L., 2002a. Absorbed dose fraction for 87Rb beta particles. *Anc. TL* 20, 25–29.
- Readhead, M.L., 2002b. Appendix to “Absorbed dose fraction for 87Rb beta particles”. *Anc. TL* 20, 47.
- Rees-Jones, J., Tite, M.S., 1997. Optical dating results for British archaeological sediments. *Archaeometry* 39, 177–187.
- Rees-Jones, J., 1995. Optical dating of young sediments using fine-grained quartz. *Anc. TL* 13, 9–14.
- Ripley, B., 2013. *Pspline: Penalized Smoothing Splines. R Package Version 1.0-16. S original by Jim Ramsey.* <http://CRAN.R-project.org/package=pspline>.
- Roskosch, J., Tsukamoto, S., Meinsen, J., Frechen, M., Winsemann, J., 2012. Luminescence dating of an Upper Pleistocene alluvial fan and aeolian sandsheet complex: the Senne in the Münsterland Embayment, NW Germany. *Quat. Geochronol.* 10, 94–101.
- Schatz, A.-K., Buylaert, J.-P., Murray, A., Stevens, T., Scholten, T., 2012. Establishing a luminescence chronology for a palaeosol-loess profile at Tokaj (Hungary): a comparison of quartz OSL and polymineral IRSL signals. *Quat. Geochronol.* 10, 68–74.
- Schmidt, E.D., Tsukamoto, S., Frechen, M., Murray, A.S., 2014. Elevated temperature IRSL dating of loess sections in the East Eifel region of Germany. *Quat. Int.* 334–335, 141–154.
- Schokker, J., Cleveringa, P., Murray, A.S., Wallinga, J., Westerhoff, W.E., 2005. An OSL dated middle and late quaternary sedimentary record in the Roer Valley Graben (southeastern Netherlands). *Quat. Sci. Rev.* 24, 2243–2264.
- Smedley, R.K., Duller, G.A.T., Pearce, N.J.G., Roberts, H.M., 2012. Determining the K-content of single-grains of feldspar for luminescence dating. *Radiat. Meas.* 47, 790–796.
- Spooner, N.A., Aitken, M.J., Smith, B.W., Franks, M., McElroy, C., 1990. Archaeological dating by infrared-stimulated luminescence using a diode array. *Radiat. Prot. Dosim.* 34, 83–86.
- Stevens, T., Markovic, S.B., Zech, M., Hambach, U., Sumegi, P., 2011. Dust deposition and climate in the Carpathian Basin over an independently dated last glacial-interglacial cycle. *Quat. Sci. Rev.* 30, 662–681.
- Sutton, S.R., Zimmerman, D.W., 1978. Thermoluminescence dating: radioactivity in quartz. *Archaeometry* 20, 66–88.
- Tamura, T., Bateman, M.D., Kodama, Y., Saitoh, Y., Watanabe, K., Yamaguchi, N., Matsumoto, D., 2011. Building of shore-oblique transverse dune ridges revealed by ground-penetrating radar and optical dating over the last 500 years on Tottori coast, Japan Sea. *Geomorphology* 132, 153–166.
- Thiel, C., Buylaert, J.-P., Murray, A.S., Terhorst, B., Hofer, B., Tsukamoto, S., Frechen, M., 2011. Luminescence dating of the Stratzing loess profile (Austria) – testing the potential of an elevated temperature post-IR IRSL protocol. *Quat. Int.* 234, 23–31.
- Thomsen, K.J., Murray, A.S., Jain, M., Bøtter-Jensen, L., 2008. Laboratory fading rates of various luminescence signals from feldspar-rich sediment extracts. *Radiat. Meas.* 43, 1474–1486.
- Vandenbergh, D., De Corte, F., Buylaert, J.-P., Kučera, J., Van Den Haute, P., 2008. On the internal radioactivity in quartz. *Radiat. Meas.* 43, 771–775.
- Xu, L., Ou, X., Lai, Z., Zhou, S., Wang, J., Fu, Y., 2010. Timing and style of Late Pleistocene glaciation in the Queer Shan, northern Hengduan Mountains in the eastern Tibetan Plateau. *J. Quat. Sci.* 25, 957–966.
- Yang, L., Zhou, J., Lai, Z., Long, H., Zhang, J., 2010. Late glacial and Holocene dune evolution in the Horqin dunefield of northeastern China based on luminescence dating. *Palaeogeogr. Palaeoclimatol. Palaeoecol.* 296, 44–51.
- Zimmerman, D.W., 1971. Thermoluminescent dating using fine grains from pottery. *Archaeometry* 13, 29–52.